Metallophysics and Advanced Technologies
Металофіз. новітні технол.
Metallofiz. Noveishie Tekhnol.
2025, vol. 47, No. 3, pp. 303–333
https://doi.org/10.15407/mfint.47.03.0303
Reprints available directly from the publisher

PACS numbers: 46.35.+z, 61.72.Bb, 61.72.Lk, 62.20.fg, 81.40.Cd, 83.60.La

The Effect of the Shear-Stress Field in the Glide Plane on Solid Solution Strengthening in Multicomponent Alloys

M. I. Lugovyy, D. G. Verbylo, and M. P. Brodnikovskyy

I. M. Frantsevych Institute for Problems in Materials Science, N.A.S. of Ukraine,
3, Omeljan Pritsak Str.,
UA-03142 Kyiv, Ukraine

Atomic-sizes' misfit and elastic-moduli misfit for the solute atoms at the crystal-lattice sites in concentrated solid solution, notably, in multicomponent alloy, can be considered as discrete random variables. Definition of variance of such random variables allows to develop method and analytical expressions to determine the main parameters of stochastic shearing-stresses' field that is generated within the glide plane by solute atoms. The main parameters are the standard deviations and correlation lengths of the short- and long-wavelength components of this field. The developed method also shows that it is possible to determine two different effective distortions of crystal lattice, each of which is responsible for its own component of the shearing-stresses' field. Another conclusion of the new method is that there is no single empirical constant for all alloys at once to determine the yield strength using the shear modulus and average lattice distortion. The short-wavelength component of the shearing-stresses' field within the glide plane creates dominant force barriers, which the dislocation can overcome by the thermal-activation assistance. The long-wavelength component creates barriers, which can be overcome athermally, that is, by applying additional mechanical stress. All these barriers can be described using the main parameters of the shearing-stresses' field. Effect of solute atoms located farther from the glide plane on yield strength cannot be neglected because they create long-wavelength component of the shearing-stresses' field. The analysis of

Corresponding author: Mykola Ivanovych Lugovyy
E-mail: m.lugovyi@ipms.kyiv.ua

Citation: M. I. Lugovyy, D. G. Verbylo, and M. P. Brodnikovskyy, The Effect of the Shear Stress Field in the Glide Plane on Solid Solution Strengthening in Multicomponent Alloys, *Metallofiz. Noveishie Tekhnol.*, **47**, No. 3: 303–333 (2025). DOI: 10.15407/mfint.47.03.0303

overcoming barriers from the short- and long-wavelength components of the shearing-stresses' field is resulted in describing the temperature dependence of the yield strength of a multicomponent alloy. This dependence describes well the mechanical behaviour of the alloy in a wide range of temperatures, including in the range of the high-temperature 'plateau', except very low and very high temperatures, where additional factors and mechanisms operate.

Key words: multicomponent alloy, solid solution, glide plane, shearing stresses, dislocation, yield strength.

Невідповідності атомових розмірів і модулів пружности для розчинених атомів у вузлах кристалічних ґратниць концентрованого твердого розчину, який являє собою багатокомпонентний стоп, можна розглядати як дискретні випадкові величини. Визначення дисперсії цих випадкових величин уможливлює розробити метод розрахунку й одержати аналітичні вирази для основних параметрів поля стохастичних зсувних напружень, яких зґенеровано у площині ковзу розчиненими атомами. Основними параметрами є стандартні відхили та довжини кореляції коротко- та довгохвильової компонент цього поля. Розроблений метод також показує, що можна визначити дві різні ефективні дисторсії кристалічних ґратниць, кожна з яких відповідає за свою компоненту поля зсувних напружень. Ще один висновок нового методу: немає єдиної емпіричної константи одразу для всіх стопів, щоб визначити границі плинности через модуль зсуву та середню дисторсію ґратниць. Короткохвильова компонента поля зсувних напружень у площині ковзу створює домінантні силові бар'єри, які дислокація може долати за допомогою термічної активації. Довгохвильова компонента створює бар'єри, які можуть бути подолані атермічно, тобто шляхом прикладання додаткового механічного напруження. Всі ці бар'єри можна описати за допомогою основних параметрів поля зсувних напружень. Не можна нехтувати впливом атомів розчиненої речовини, розташованих далі від площини ковзу, на границю плинности, оскільки вони створюють довгохвильову компоненту поля зсувних напружень. Аналіза подолання бар'єрів від коротко- та довгохвильової компонент поля зсувних напружень дає нам температурну залежність границі плинности багатокомпонентного стопу, яка може добре описати механічну поведінку стопу в широкому діяпазоні температур, в тому числі й в області високотемпературного «плато», за винятком дуже низьких і дуже високих температур, де діють додаткові чинники та механізми.

Ключові слова: багатокомпонентний стоп, твердий розчин, площина ковзу, зсувні напруження, дислокації, межа плинности.

(Received 6 June, 2024; in final version, 14 October, 2024)

1. INTRODUCTION

Multicomponent alloys are promising materials that demonstrate many unique properties, in particular, very high yield strengths [1, 2]. The yield strength of such alloys, which are mostly substitutional solid

solutions, depends on the distribution of internal stresses in the material. It should be noted that the distribution of internal stresses affects the shape of the dislocation line, which also affects the stress required to start its movement in the glide plane [3]. Solid solution strengthening allows achieving high yield strength in multicomponent alloys even at high temperatures. Thus, the concept of solid solution strengthening allows obtaining materials for applications in a wide range of temperatures [1]. Such features of the mechanical behaviour of these materials are very useful for use in modern technology [1, 2].

Crystal lattice distortion created by solute atoms results in stochastic shear stresses in the dislocation glide plane. The different atoms in the solid solution have some atomic size misfit and elastic modulus misfit in comparison with the average atomic size and the effective elastic modulus of the alloy. These misfits lead to distortion of the crystal lattice, which varies randomly in space. Local distortion changes with temperature, and understanding the features of these changes is important for determining the temperature dependence of the material's yield strength. In such a way, crystal lattice distortion is a source of internal stresses. In the case of alloys where there is no dominant component, the internal shear stress at any point of glide plane is a random variable, which typically has a statistical distribution according to the normal law, because these stresses are the sum of contributions of many solute atoms, which are located around the glide plane. In general, these internal stresses follow a zero balance, that is, the stress averaged over the entire glide plane must be zero. Regions with stresses of different signs alternate with each other on the glide plane, which results in a zero balance of forces. The average size of the region where the stresses have the same sign is an important characteristic of the stochastic shear-stress field, which determines its correlation length. These stresses lead to forces acting on the dislocation, affecting its shape, and creating resistance to its movement due to the deviation of dislocation shape from a straight line. The wavy equilibrium shape of the dislocation is formed by the balancing of the forces acting on individual segments of the dislocation due to shear-stress field and the forces of linear tension, which in turn depend on the shape of the dislocation line. Thus, this shape is a set of ‘waves’, *i.e.*, bulges of different lengths and heights. To estimate the parameters of the average bulge, the first step is to determine idealized shape of the bulge.

One of such attempts was the consideration of the quadratic parabolic form of such bulge [3]. The use of the shape of an arc of a circle is also quite widespread [4]. For bulges, in which the height is much smaller than the length, these two idealized shapes give the same numerical results. In a numerical experiment using the method of discrete dislocation dynamics, it was found that the best approximation for the shape

of the average bulge of the dislocation line will be a sinusoidal shape, in which the wave height is also much smaller than its length [5].

Modelling of solid solution strengthening and yield strength of multicomponent alloys, which is important for the development of new alloys, was considered in many works [3, 6–22]. In particular, the effect of the dislocation line shape in solid solution on the yield point was studied in [3, 6–19]. Such modelling allows predicting the likely yield strengths of such materials and can help in the development of new promising alloys of this class [3, 6–28]. Many works were devoted to the theoretical description of solid solution strengthening and the corresponding formation of the temperature dependence of the yield strength [3, 6–31]. In work [3], the critical stress necessary for the start of dislocation motion in the stochastic shear-stress field in the glide plane, essentially the yield point, is considered. The amplitude of the shear stresses, the average linear size of the region, where the stochastic stresses have the same sign, and the length of the dislocation segment, where the elementary-gliding process occurs, *i.e.*, the length of the average bulge on the dislocation line, are important in this case. The paper [6] considered the interaction of a moving dislocation with obstacles in the glide plane, which are created by solute atoms located in the immediate vicinity of this plane. There are two types of dislocation interaction with obstacles in the glide plane. The first type is when these obstacles can be considered as points. It is true for very dilute solid solutions, in which there are few solute atoms, which are located at a large distance from each other [32]. The second type is when the obstacles have a finite range of interaction with the dislocation, *i.e.* a certain size in the direction of dislocation motion, and the statistics of the interaction of the dislocation with such obstacles are different from the first case [3].

A new theory to calculate the yield strength of disordered solid solutions with an arbitrary number of components and an arbitrary composition, based on the Labusch model, was proposed in [7–15]. In these works, the waviness and roughness of the dislocation line were modelled in a simplified form by the identical trapezoidal protrusions in two opposite directions lying in the glide plane. The height and length of the protrusions were determined by first-principles calculations using density functional method. This theory uses the calculated first-principles interaction energies of solute atoms with dislocations as inputs to determine the yield strength and activation volume as functions of composition, temperature, and strain rate. Reducing waviness to uniform trapezoidal ridges requires neglecting the actual shape of the dislocation line, which is actually a sum of bulges of different heights, lengths, and shapes. Besides, one-dimensional sinusoidal dependence of internal stresses on the coordinate along the direction of dislocation motion was only considered in this theory. Neglecting the

real two-dimensional stochastic distribution of shear stresses in the glide plane can lead to significant errors in determining the shape of the dislocation line and the yield strength of the material.

The dislocation line shape was modelled using discrete dislocation dynamics [17]. Such modelling gives a more realistic shape, but it depends on the method of determining the stochastic shear-stress field in the glide plane. To model the distribution of shear stresses, a special method was developed in [17]. The force acting from the shear-stress field on a certain dislocation segment was calculated as a superposition of forces from randomly located pinning points in the glide plane, each of which created a Gaussian pinning potential. At the same time, the force acting on the dislocation from a certain pinning point dropped to almost zero when moving away from this point. Thus, pinning points located far from the dislocation segment practically did not act on it. This way of determining the forces acting on the dislocation and actually determining the shear-stress field provides a normal distribution of probabilities for these stresses, since the stress at a certain point is the sum of many random small contributions from different pinning points. However, this method has its drawbacks. First, the variance of the normal distribution is poorly specified by this method, as it depends on the number of pinning points that fall into the zone of influence around a certain point on the dislocation line. It should also be noted that the pinning points, which contribute to the force acting on a certain point on the dislocation line, are located only in the glide plane in the method proposed in [17]. However, in a real alloy, many crystal lattice distortion centres, which will contribute to the stochastic shear-stress field in the glide plane, are located in the space above and below the glide plane.

It should be noted that namely with such a more realistic approach, the distribution of shear stresses in the glide plane is divided into short-wavelength and long-wavelength components. Second, the identical pinning points are more consistent with modelling a binary alloy in which the identical solute atoms are dissolved in the solvent matrix. This method is somewhat questionable for multicomponent alloys. Thirdly, this method requires significant computing power and time spent on calculations. Thus, the development of another method of determining stochastic shear stresses in the glide plane may be useful. In addition, an insufficiently accurate method for determining the characteristic parameters of the dislocation line shape was proposed in [17], and the statistics of the various components of this shape were not studied.

Since the dislocation line shape was modelled only at zero applied stress in Ref. [17], the question arises about the evolution of this shape under the action of an external load. It was also noted that, in order to determine directly the yield strength using such modelling, it is neces-

sary to find such a critical applied stress at which the dislocation line shape ceases to be in equilibrium. In this case, the velocities of all segments of the dislocation will not go to zero sometime after the application of this external stress. Therefore, the dislocation will not stop and not reach an equilibrium shape. Such determination of yield strength requires successively increasing the applied stress from zero with a certain small step and checking the equilibrium shape of the dislocation line at each such step. The segments of the dislocation start to move with each subsequent increased stress, because their equilibrium is disturbed. Further, two cases are possible. First, the dislocation segments may stop after some time. This will mean that new equilibrium shape has been reached. Second, the movement of the segments will not stop and the dislocation will break away from the points of initial pinning. This can be conventionally considered as the plastic deformation beginning.

Various aspects of thermal activation analysis of the temperature dependence of the yield strength in binary and multicomponent solid solutions, in particular in high-entropy alloys, were considered in [25-28]. One of the considered problems is the existence of a 'plateau' on the temperature dependence of the critical shear stress at high temperatures, an almost constant value of the yield strength in a certain temperature range. The paper [25] shows that the existence of such a 'plateau' is essentially anomalous. The elastic modulus of the material decreases as the temperature increases, which in turn should lead to a decrease in the stochastic shear stresses in the dislocation glide plane, which are created by numerous local distortions of the crystal lattice, and, accordingly, to a decrease in the yield strength, rather than its constant value at elevated temperatures. Since the 'plateau' is observed experimentally, there must be additional factors that compensate for the decrease in the elastic modulus with increasing temperature. In particular, the drop in the shear modulus must be compensated by an increase in the distortion of the crystal lattice as the temperature increases for the 'plateau' existence. In the temperature region, where a 'plateau' is observed, in multicomponent solid solutions, in addition to an increase in the root mean square displacements of atoms, there may also be an effect of dynamic deformation ageing accompanied by the corresponding strengthening, which compensates for the elastic modulus decrease [25]. However, this effect is not universal and cannot explain the 'plateau' in all cases. Thus, the factors that compensate for the elastic modulus decrease due to the increase in temperature and contribute to the emergence of a 'plateau' require further research. The study of the dependence of the crystal lattice distortion on temperature is relevant in this sense.

Some issues of determining lattice distortion and yield strength in multicomponent alloys were discussed in Refs. [20–22]. Modelling of

dislocation motion by the method of discrete dislocation dynamics and calculation of the stochastic shear-stress field in the glide plane by direct summation of contributions from individual solute atoms located at the sites of crystal lattice in the space around this plane are considered in Refs. [5, 23, 24, 33]. The shear stress acting on the edge dislocation in the glide plane from a single solute atom can be calculated using the energy of interaction of such an atom and a trial rectilinear segment of the dislocation [24]. It should be noted that each atom in the substitutional solid solution could be considered as a point defect in the effective averaged matrix-solvent media [11, 12, 20–22]. The zone of influence of such a defect on the dislocation in the glide plane is greater the farther this defect is from the plane, but the interaction force decreases in this case [34]. Thus, the stochastic shear-stress field, which is created by solute atoms in the glide plane in a multicomponent alloy, can be divided into two components. The short-wavelength component with a larger amplitude and shorter correlation length of the stress field is created by solute atoms located in the immediate vicinity of the glide plane. For example, in Ref. [4], it is proposed to take into account affecting of only these atoms to the dislocation motion. The long-wavelength component with a much smaller amplitude and longer correlation length is created by atoms, which are farther from the glide plane. Typically, this component is neglected, but it can be quite significant. It can be supposed that the short-wavelength component of the shear-stress field is related to the thermal component of solid solution strengthening of multicomponent alloy. The long-wavelength component can be tried to be related to the athermal component of this strengthening, because its significantly longer correlation length can prevent thermally activated overcoming of energy barriers, which associated with it [34].

The characteristics of the shear-stresses' distribution in the glide plane in a solid solution can be calculated both by direct summation of contributions from many solute atoms [24, 33] and by using a special statistical method [35]. The main parameters of this distribution are the standard deviation and the correlation length of the short-wavelength component of the stochastic shear-stress field in the glide plane and the standard deviation and the correlation length of its long-wavelength component. The shear-stresses' distribution is the main factor in modelling dislocation motion in the glide plane by the method of discrete dislocation dynamics [5, 23]. In particular, such simulation shows the reality of the sequential action of the short- and long-wavelength components of the shear-stress field on the dislocation motion. This also clarifies the sinusoidal shape of the bulges on the dislocation line. These bulges are formed and disappear under the action of an external load, and the dislocation moves ahead by such a way.

The equilibrium shape of the dislocation at zero load fits well into a

band with a width of three full correlation lengths of the short-wavelength component of the shear-stress field [5]. The waviness of the dislocation line on the scale of the correlation length of the long-wavelength component does not appear without an external load. The external stress applied in the glide plane, which assists the dislocation segments to overcome the internal force barriers, can, to some extent, compensate for the short-wavelength component of the shear-stress field. Then, the waviness of the dislocation line will be activated on the scale that is associated with the long-wavelength component as the numerical experiment shows. Thus, the two components of the shear-stress field affect the dislocation line shape separately and sequentially when the external load increases. It is relevant to study how the two components of the shear-stress field affect the temperature dependence of the yield strength of a multicomponent alloy.

The goal of this work is to consider the statistical method of determining the characteristics of the stochastic shear-stress field in the glide plane in a multicomponent alloy and the influence of these characteristics on the temperature dependence of the yield strength in such an alloy, taking into account the short- and long-wavelength components of this field.

2. CALCULATION ALGORITHMS

2.1. Determination of Characteristics of Stochastic Shear-Stresses' Field in Glide Plane in Multicomponent Alloy

Shear stress τ_s that acts to trial rectilinear segment of the dislocation with the coordinates of centre x_u and z_u in the glide plane from solute atoms, which are located at the sites of crystal lattice with coordinates x_{hkm}, y_{hkm}, z_{hkm} in the space around this plane in multicomponent alloy, and gradient of this stress g_x along the x axis can be calculated as sums of contributions from these atoms [24, 33, 35]:

$$\tau_s = \sum_h \left(\sum_k \left(\sum_m \left(\frac{Gp'_{hkm} V_a}{b\Delta z} \tilde{\Delta} + \frac{Gq'_{hkm} V_a}{b\Delta z} \tilde{H} \right) \right) \right), \tag{1a}$$

$$g_x = \frac{\partial \tau_s}{\partial x} = \sum_h \left(\sum_k \left(\sum_m \left(\frac{Gp''_{hkm} V_a}{b\Delta z} \tilde{\Delta} + \frac{Gq''_{hkm} V_a}{b\Delta z} \tilde{H} \right) \right) \right). \tag{1b}$$

where G is the shear modulus of the alloy, b is the absolute value of Burgers vector of the alloy, V_a is the volume per atom for the alloy ($V_a = b^3(2)^{-1/2}$ for the alloy with f.c.c. lattice, $V_a = 4b^3/(3(3)^{1/2})$ for the alloy with b.c.c. lattice), Δz is the length of trial rectilinear segment of the edge dislocation, h, k and m are the indices, which specify the coor-

dinates of the sites where the solute atoms are located, along the axes x (in the glide plane in the direction of dislocation motion), y (perpendicular to the glide plane) and z (in the glide plane along the dislocation line) [24], h is the number of the plane perpendicular to the Burgers vector, in which the site is located, k is the number of the atomic row in the plane in which the site is located, m is the site number in the atomic row, $\tilde{\Delta}$ and $\tilde{H}$ are the discrete random variables that determine the atomic size misfit and elastic modulus misfit of a solute atom at a crystal lattice site in comparison with the 'average' atoms of a virtual matrix-solvent, respectively, and since an atom of any component can be located in a given site with a certain probability, then these variables take on their individual values for each site, p'_{hkm}, q'_{hkm}, p''_{hkm}, and q''_{hkm} are the variables that are related to the first and second derivatives of both pressure and energy density of elastic deformations by the x coordinate, respectively. The pressure and energy density are created by a trial segment of the edge dislocation at the point, where the solute atom is located.

If we sum in (1) only the contributions of the solute atoms in the two atomic planes nearest to the glide plane on each side, then this will be the so-called short-wavelength component τ_{s1} of the shear-stress field and its gradient g_{x1} [35]. The long-wavelength component of the shear-stress field τ_{s2} and its gradient g_{x2} are easily calculated from the equations [35]:

$$\tau_{s2} = \tau_s - \tau_{s1} \text{ and } g_{x2} = g_x - g_{x1}. \qquad (2)$$

The region of the dislocation core, where the elastic behaviour of the material is disturbed, should also be taken into account. This means that contributions of solute atoms located in the region of the dislocation core

$$\sqrt{(x_{hkm} - x_u)^2 + y_{hkm}^2} \le r_c, \left|z_{hkm} - z_u\right| \le \Delta z / 2,$$

where r_c is the radius of the dislocation core ($r_c \approx b$ for f.c.c. lattice), to the shear stress in the glide plane and to its gradient can be neglected, *i.e.*, equate to zero the corresponding terms in Eqs. (1). Contributions of solute atoms, which are far enough from the point of shear-stress determination at a distance greater than a certain critical distance, become very small and can be neglected too. Thus, the summation should be carried out, taking into account only the sites located at a distance that is less than the critical distance.

Variables $\tilde{\Delta}$ and $\tilde{H}$ can take the values of δ_i and η'_i with the probability X_i, respectively, where $\delta_I = (1/s_{lat})(ds_{lat}/dX_i)$ is the atomic size misfit of the component i in comparison with the atoms of the virtual effective averaged matrix-solvent (a conventional material consisting

of 'average' atoms of a solid solution [11]), s_{lat} is the average distance between the nearest atoms in the alloy ($s_{\text{lat}} = b$), $\eta'_i = \eta_i / (1 + 0.5|\eta_i|)$, $\eta_i = (1/G)(dG/dX_i)$ is the elastic modulus misfit of the component i in comparison with the atoms of the matrix-solvent [24, 33], X_i is the atomic fraction of the component i (note that the sum of the atomic fractions of all components is equal to one, that is, the sum of the probabilities of all possible options will, as it should, also be equal to one). Mathematical expectations of discrete random variables $\tilde{\Delta}$ and $\tilde{H}$ will be equal to zero due to the balance of positive and negative misfits:

$$E(\tilde{\Delta}) = \sum_{i=1}^{N} \delta_i X_i = 0 \text{ and } E(\tilde{H}) = \sum_{i=1}^{N} \eta'_i X_i = 0 .$$

In this case the variances of the variables $\tilde{\Delta}$ and $\tilde{H}$ are

$$D(\tilde{\Delta}) = \sum_{i=1}^{N} \delta_i^2 X_i \text{ and } D(\tilde{H}) = \sum_{i=1}^{N} (\eta'_i)^2 X_i ,$$

respectively.

Taking into account the details of the calculation of shear stresses given in Ref. [24], the variables p'_{hkm}, q'_{hkm}, p''_{hkm}, and q''_{hkm} can be determined through the numerically calculated first and second derivatives of both the pressure and the energy density of elastic deformations by the x coordinate, respectively [35]:

$$p'_{hkm} = 3\frac{p^{(1)}_{hkm} - p^{(2)}_{hkm}}{G\Delta x}, \tag{3a}$$

$$q'_{hkm} = \frac{q^{(1)}_{hkm} - q^{(2)}_{hkm}}{G\Delta x}, \tag{3b}$$

$$p''_{hkm} = \frac{6p^{(1)}_{hkm} - 3(p^{(2)}_{hkm} + p^{(3)}_{hkm})}{G\Delta x^2}, \tag{3c}$$

$$q''_{hkm} = \frac{2q^{(1)}_{hkm} - q^{(2)}_{hkm} - q^{(3)}_{hkm}}{G\Delta x^2}, \tag{3d}$$

where Δx is the small step along the x coordinate in the direction that is perpendicular to the trial segment of the edge dislocation (it is appropriate to accept $\Delta x = b/100$ [24, 33]);

$$p^{(j)}_{hkm} = -\frac{\sigma_{xx} + \sigma_{yy} + \sigma_{zz}}{3} \tag{4a}$$

is the pressure that is created by a trial segment of the edge dislocation with the coordinates of centre z_u and x_u ($j = 1$), $x_u + \Delta x$ ($j = 2$), $x_u - \Delta x$ ($j = 3$) at the point with the coordinates x_{hkm}, y_{hkm}, z_{hkm} [35];

$$q_{hkm}^{(j)} = \frac{(p_{hkm}^{(j)})^2}{2K} + \frac{\sigma_{xy}^2 + \sigma_{xz}^2 + \sigma_{yz}^2}{2G} \quad (4b)$$

is the energy density of elastic deformations in this point, σ_{xx}, σ_{yy}, σ_{zz}, σ_{xy}, σ_{xz}, σ_{yz} are the stress tensor components for the stress created by a trial segment of the edge dislocation at the point where the solute atom is located (details of the calculation of stress tensor components are given in Ref. [24]), K is the bulk modulus of the alloy.

The shear stress at a local point of the glide plane and gradient of this stress in the multicomponent alloy will be normally distributed random variables because, in accordance with (1), they will be the sums of a large number of random variables. Each of the variables is determined for its own site and multiplied by the corresponding constant. This was confirmed in shear-stress calculation by direct summation of contributions from individual solute atoms [24]. The mathematical expectations and variances of such normally distributed variables will be equal to the sums of the mathematical expectations and variances of summed random variables, which are multiplied by certain coefficients, respectively. Mathematical expectations of shear stress and gradient of this stress will be equal to zero due to the fact that $E(\tilde{\Delta}) = 0$ and $E(\tilde{H}) = 0$, that is, all components of mathematical expectations and their sum are equal to zero. This corresponds to the condition of zero balance of shear stresses in the glide plane and is confirmed by direct summation of contributions [24].

Taking into account the definition of the variances of discrete random variables $\tilde{\Delta}$ and $\tilde{H}$, the variance of the shear stress and gradient of this stress are, respectively [35]:

$$D(\tau_s) = s^2 = \sum_h \left(\sum_k \left(\sum_m \left[\left(\frac{Gp'_{hkm} V_a}{b\Delta z} \right)^2 D(\tilde{\Delta}) + \left(\frac{Gq'_{hkm} V_a}{b\Delta z} \right)^2 D(\tilde{H}) \right] \right) \right), \quad (5a)$$

$$D(g_x) = s_g^2 = \sum_h \left(\sum_k \left(\sum_m \left[\left(\frac{Gp''_{hkm} V_a}{b\Delta z} \right)^2 D(\tilde{\Delta}) + \left(\frac{Gq''_{hkm} V_a}{b\Delta z} \right)^2 D(\tilde{H}) \right] \right) \right), \quad (5b)$$

where s and s_g are the standard deviations of the shear stress and gradient of this stress, respectively. These deviations, as well as, by analogy, the corresponding deviations for the short- and long-wavelength components and corresponding gradients, s_1, s_{g1}, s_2, s_{g2}, can be expressed from (5) after some transformations taking into account the definition of $D(\tilde{\Delta})$ and $D(\tilde{H})$ as follows [35]:

$$s = \frac{GV_a}{b\Delta z} (Q')^{1/2} \left(\sum_{i=1}^{N} (\eta_i'^2 + \alpha_s^2 \delta_i^2) X_i \right)^{1/2}, \quad (6a)$$

$$s_g = \frac{GV_a}{b\Delta z}(Q'')^{1/2}\left(\sum_{i=1}^{N}(\eta_i'^2 + \alpha_g^2\delta_i^2)X_i\right)^{1/2}, \tag{6b}$$

$$s_1 = \frac{GV_a}{b\Delta z}(Q_1')^{1/2}\left(\sum_{i=1}^{N}(\eta_i'^2 + \alpha_{s1}^2\delta_i^2)X_i\right)^{1/2}, \tag{6c}$$

$$s_{g1} = \frac{GV_a}{b\Delta z}(Q_1'')^{1/2}\left(\sum_{i=1}^{N}(\eta_i'^2 + \alpha_{g1}^2\delta_i^2)X_i\right)^{1/2}, \tag{6d}$$

$$s_2 = \frac{GV_a}{b\Delta z}(Q_2')^{1/2}\left(\sum_{i=1}^{N}(\eta_i'^2 + \alpha_{s2}^2\delta_i^2)X_i\right)^{1/2}, \tag{6e}$$

$$s_{g2} = \frac{GV_a}{b\Delta z}(Q_2'')^{1/2}\left(\sum_{i=1}^{N}(\eta_i'^2 + \alpha_{g2}^2\delta_i^2)X_i\right)^{1/2}, \tag{6f}$$

where

$$\alpha_s = (P'/Q')^{1/2} \text{ and } \alpha_g = (P''/Q'')^{1/2}, \tag{7a}$$

$$\alpha_{s1} = (P_1'/Q_1')^{1/2} \text{ and } \alpha_{g1} = (P_1''/Q_1'')^{1/2}, \tag{7b}$$

$$\alpha_{s2} = (P_2'/Q_2')^{1/2} \text{ and } \alpha_{g2} = (P_2''/Q_2'')^{1/2}, \tag{7c}$$

$$P' = \sum_h\left(\sum_k\left(\sum_m (p'_{hkm})^2\right)\right) \text{ and } P'' = \sum_h\left(\sum_k\left(\sum_m (p''_{hkm})^2\right)\right), \tag{8}$$

and

$$Q' = \sum_h\left(\sum_k\left(\sum_m (q'_{hkm})^2\right)\right) \text{ and } Q'' = \sum_h\left(\sum_k\left(\sum_m (q''_{hkm})^2\right)\right). \tag{9}$$

Parameters P_1', P_1'', Q_1', Q_1'' for short-wavelength component can be obtained, if we sum up the contributions only from solute atoms in the two atomic planes nearest to the glide plane on each side. The parameters for the long-wavelength component are calculated as $P_2' = P' - P_1'$, $Q_2' = Q' - Q_1'$, $P_2'' = P'' - P_1''$, and $Q_2'' = Q'' - Q_1''$.

It is also important to determine the correlation lengths w_1 and w_2 of the short- and long-wavelength components of the stochastic shear-stress field in the glide plane, *i.e.* the average linear dimensions of regions where the short-wavelength component has the same sign and regions where the long-wavelength component has the same sign. The distribution of positive shear stresses along the axis inside such a region will be considered, regardless of the component, to do this. Schematically, three individual realizations of such shear-stresses' distribution as random variable are shown in Fig. 1. The points that are located exactly in the middle between the endpoints of the distributions are combined together. This centre point is chosen as the coordinate

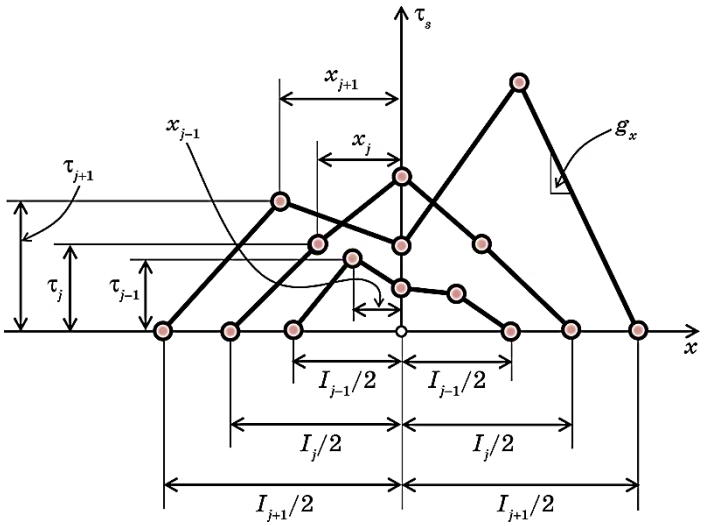

Fig. 1. Schematic presentation of three individual realizations of the distribution of positive shear stresses as random variables [35]. Grey circles show the corresponding random values.

origin. First, for these realizations, as well as all similar ones, the shear stress is always zero at the endpoints. Secondly, the size of the regions and the maximum stress in the regions may be different for different realizations. Thirdly, different realizations can have several local maxima and be completely asymmetric. However, it is possible to determine the average stress distribution for such regions. The size of the region of such an average distribution will be equal to, by definition, the average linear size of the region where the stresses are positive, *i.e.* the correlation length $w = <l_j>$, where l_j is the size of the region of the j-th realization.

If shear stress, as random variable, have a normal distribution with zero mathematical expectation and standard deviation s, then a set of only positive values from such distribution has an average value, which will be the average stress value of $m_s = <\tau_j> = s(2/\pi)^{1/2}$ for our average distribution. If the special coordinates $(x_j/l_j)w$ for each realization will be defined, then, the points of all realizations can be displayed in single average region with the size w. Further, it is possible to average the stress over all realizations for each special coordinate $(x_j/l_j)w$ and obtain the average distribution of positive stresses in the region with the size w (Fig. 2). The stresses of the average distribution will be equal to zero at the end points of the region. Further, the stress should increase from each end point towards the centre of the region, since the average stress value of the average distribution is greater than zero. This increase will be symmetrical relative to the centre point of the region be-

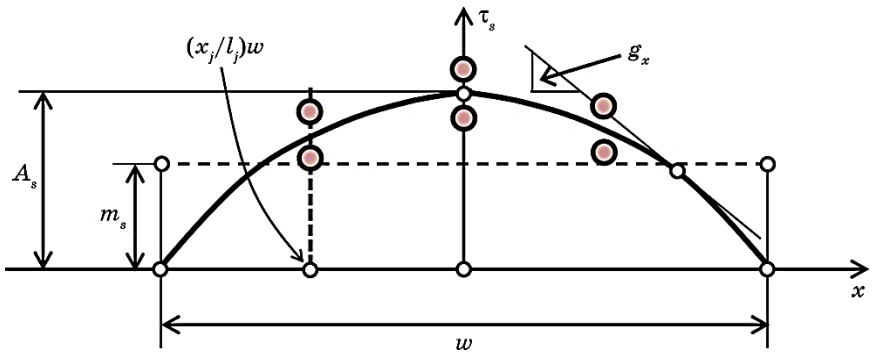

Fig. 2. Schematic presentation of the averaged distribution of positive shear stresses as random variables [35]. Grey circles show the corresponding random values.

cause the portions of the region on both sides of the centre point are absolutely equal and have no advantages over each other due to the homogeneity of the statistical distribution of stresses on the glide plane. Thus, the average distribution will be a smooth curve symmetrical relative to the centre point with the maximum at this point. Note that the average value of the stress gradient for the average distribution will be zero, because the stress must rise from zero at one end point and fall to zero at the other. The change in the gradient along the average distribution region is shown in Fig. 3. If only the positive values of the gradient will be averaged, then, similarly to the stress, we will have an average value of $m_g = s_g(2/\pi)^{1/2}$. The average distribution can be approximated by a suitable function, for example $\tau_s = A_s\cos(\pi x/w)$ or $\tau_s = A_s(1 - |2x/w|^n)$, where n is the exponent ($n > 1$). Then maximum values of average distribution will be $A_s = \pi m_s/2$ and $A_s = (n+1)m_s/n$ for these approximation functions, respectively (Fig. 2). If the stress gradient for both functions is averaged over the portion where it is positive, a single result for average gradient of $m_g = 2A_s/2$ is obtained (Fig. 3). Further, it is easy to derive expressions for w and, by analogy, for w_1 and w_2 for both approximation functions [35]:

$$w = \pi s / s_g,\ w = 2(n+1)s / (ns_g), \tag{10a}$$

$$w_1 = \pi s_1 / s_{g1},\ w_1 = 2(n+1)s_1 / (ns_{g1}), \tag{10b}$$

$$w_2 = \pi s_2 / s_{g2},\ w_2 = 2(n+1)s_2 / (ns_{g2}). \tag{10c}$$

Note that, for $n = 2$, both functions result in very close results. Besides, the parameters s_1, s_{g1}, s_2 and s_{g2} depend on Δz. Besides, it was found that we should use $\Delta z = 2w_2$ [5, 36]. If Eqs. (10) are taken into account, it is possible to obtain, in particular, the equation

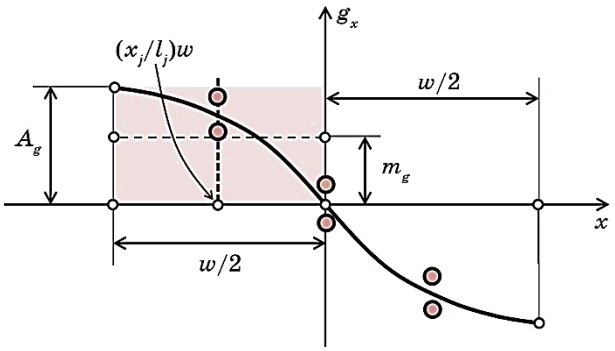

Fig. 3. Schematic presentation of the gradient of the averaged distribution of positive shear stresses as random variables [35]. Grey circles show the corresponding random values.

$w_2 = \pi s_2(2w_2)/s_{g2}(2w_2)$ allowing to determine the values of Δz and w_2.

The main parameters of the stress field may also depend on the coordinates x_u and z_u. At the same time, it should be taken into account that, for convenience, the origin of coordinates can be chosen so that it lies in the glide plane and the nearest crystal lattice site is directly above it (in the positive direction of the y axis). Due to the periodicity of crystal lattice, the results will be repeated with the period b (distance between lattice sites in the direction of dislocation motion) for x_u and with periods $b(3)^{1/2}$ or $2b(2)^{1/2}$ (distance between sites along the dislocation line for f.c.c. and b.c.c. lattices, respectively) for z_u. Therefore, it is enough to average the main parameters of the shear-stress field in the local region of the glide plane, where $0 \le x_u \le b$ and $0 \le z_u \le b(3)^{1/2}$ or $0 \le z_u \le 2b(2)^{1/2}$, to obtain an averaged result for the entire plane. In this way, four main parameters of the stochastic shear-stress field in the glide plane can be calculated, namely the standard deviation S_1 and the correlation length w_1 of the short-wavelength component and the standard deviation S_2 and the correlation length w_2 of long-wavelength component of the stress field [35].

2.2. Temperature Dependence of Yield Strength of Multicomponent Alloy

If the virtual matrix-solvent is taken into account, the yield strength of a multicomponent alloy with the contribution of only solid solution strengthening can be expressed as follows [22, 36]:

$$\sigma_y = \overline{\sigma}^* + \overline{\sigma}_\mu + \Delta\sigma^* + \Delta\sigma_\mu = M\tau_y = M(\tau_P + \tau^* + \tau_\mu), \qquad (11)$$

where $\overline{\sigma}^*$ and $\overline{\sigma}_\mu$ are the thermal and athermal components of yield

strength of virtual matrix-solvent in the terms of normal stress, $\Delta\sigma^*$ and $\Delta\sigma_\mu$ is the thermal and athermal components of solid solution strengthening in the terms of normal stress, M is the Taylor factor ($M = 3.06$ for the material with f.c.c. lattice), τ_y is the critical resolved shear stress (yield strength in the terms of shear stress), $\tau_P = \overline{\sigma}^* / M$ is the Peierls–Nabarro stress of virtual matrix-solvent (also known as the lattice friction stress, which is typically equal to a few of megapascals for a material with f.c.c. lattice), $\tau^* = \Delta\sigma^*/M$ is the thermal component of the critical resolved shear stress associated with solid solution strengthening, $\tau_\mu = \Delta\sigma_\mu/M$ is the athermal component of the critical resolved shear stress associated with solid solution strengthening.

Since the virtual matrix-solvent without solid solution strengthening is in a certain way an ideal material and effect of grain boundaries presence is not considered, it essentially lacks sources of long-range internal stresses. Therefore, it can be assumed that $\overline{\sigma}_\mu = 0$.

There are three main factors that affect the dislocation motion: the periodic potential of the crystal lattice, which is responsible for the Peierls–Nabarro stress, the short-wavelength and long-wavelength components of the stochastic shear-stress field in the glide plane, which are created by solute atoms in a multicomponent alloy, if the alloy is in the form of a single-phase concentrated solid solution and only solid solution strengthening is considered [33]. The lattice potential creates a periodic distribution of stresses in the direction of dislocation motion, and as a result resistance to this movement. For example, the amplitude of such a distribution for a material with f.c.c. lattice is quite small. The distance in the direction of dislocation motion, at which these stresses are balanced, is approximately equal to the absolute value of the Burgers vector b. The short-wavelength component of the shear-stress field in the glide plane as a normally distributed random variable has a mathematical expectation that is equal to zero and a standard deviation $s_1(\Delta z)$ that depends on the length of the trial segment of the dislocation Δz used in the calculation of the stress distribution. The average linear size of the region where the stochastic stresses have the same sign for this component will be w_1. Then the full correlation length, the average linear size of the region where the stresses balance themselves, is $2w_1$ [33]. The long-wavelength component also has zero mathematical expectation and standard deviation $s_2(\Delta z)$ with full correlation length $2w_2$. The parameter Δz can be estimated from the condition that the correlation length of the long-wavelength component of the shear-stress field along the dislocation line should be equal to the one along the direction of the dislocation motion, *i.e.* $2w_2$. Therefore, it is possible to accept $\Delta z = 2w_2$ in calculations [5].

Each of the described factors can create force barriers for dislocation motion. The width of these barriers will be comparable with the Burgers vector for the periodic lattice potential and with w_1 and w_2 for

the short-wavelength and long-wavelength components of the shear-stress field, respectively. That is, the narrowest force barrier is created by the periodic lattice potential, and the widest force barrier is formed by the long-wave component of the shear-stress field. The stresses from the periodic lattice potential are balanced at a distance smaller than the average linear size of the region where the stochastic stresses have the same sign for the short-wavelength component. The stress of the short-wavelength component, in turn, is balanced at a distance smaller than the average linear size of the region where the long-wavelength component has the same sign. Such conclusions can be drawn from the results of calculations w_1 and w_2 for some alloys [33]. That is, all these force barriers act independently of each other, each on its own size scale. For example, it is shown that initially only short-wavelength component of the shear-stress field acts on the dislocation motion. Then, after overcoming the barriers from this component with the external stress assistance, the long-wavelength component of this field starts to affect this movement [5].

The height of these force barriers will be in a completely different ratio compared to their width. The force barrier due to the short-wavelength component will be the highest, while the barriers due to the other two factors will be significantly lower. Thus, barriers due to the short-wavelength component will dominate. Overcoming such a barrier by a dislocation with the assistance of externally applied stress and thermal activation will be a critical event to start the dislocation motion. The stress required to overcome the barrier from the short-wavelength component will determine the term τ^* in (11). Barriers due to the periodic lattice potential, which are much lower compared to the barriers due to the short-wavelength component, will be suppressed by the latter, since both types of barriers are superimposed on each other. Therefore, the barriers due to the periodic lattice potential can be taken into account by simply adding a constant stress τ_P to the stress that is necessary to overcome the barrier from the short-wavelength component. The barrier due to the long-wavelength component is significantly wider in the spatial dimension, lower in the force dimension and higher in the energy sense than the barrier from the short-wavelength component. Therefore, such a barrier, which is also superimposed on the barriers due to the short-wavelength component, can be overcome only athermally, without thermal activation. As in the case of barriers due to periodic lattice potential, the barriers due to the long-wavelength component can be taken into account by adding the constant stress required for their athermal overcoming to the stress for overcoming the barriers due to the short-wavelength component. The stress required to overcome the barrier due to the long-wavelength component will determine the term τ_μ in Eq. (11).

A dislocation in stochastic shear-stress field under the action of an

external load will not move as a whole. Rather, it will advance step-by-step by forming appropriate bulges on individual segments of finite length. The critical dislocation segment with a bulge that is directed against the direction of dislocation motion is first straightened under the action of external stress, and then a new bulge is formed on it that is directed in the direction of dislocation motion. As a result, bulges are formed on the adjacent segments, which are directed against the direction of dislocation motion. The process of straightening and changing the direction of the bulges takes place on these segments as well. This, in turn, brings the critical segment to a state where the bulge on it again becomes directed against the direction of dislocation motion and the whole process is repeated. Schematically, this process for the critical segment in an idealized form is shown in Fig. 4. Initially, there is the bulge *1* with length L_1 and height $2w_1$ at zero applied stress. The averaged coordinate of $x = 0$ can be attributed to it. Further, under an external stress equal to τ_{y1}, the bulge *1* is straightened to state *2*. It can be assigned the averaged coordinate of $x = 4w_1/3$, if it is assumed that the average bulge has a parabolic shape for simplification. The bulge takes the state *3* with the averaged coordinate of $x = 8w_1/3$ in the next step. Further, the bulge successively turns into state *4* and state *5*, and the process is repeated.

In order to analyse overcoming a force barrier by a dislocation with the assistance of the thermal activation, it is necessary to set the profile of the effective stress from the shear-stress field that acts on the critical segment of the dislocation in the direction of its movement in the glide plane, that is, the dependence of this stress on the averaged forward displacement x of this segment. To simplify the problem, consider the acceptable sinusoidal dependence proposed in [4]:

$$\tau_1(x) = \tau_{y1} \sin(\pi x / 2\tilde{x}), \tag{12}$$

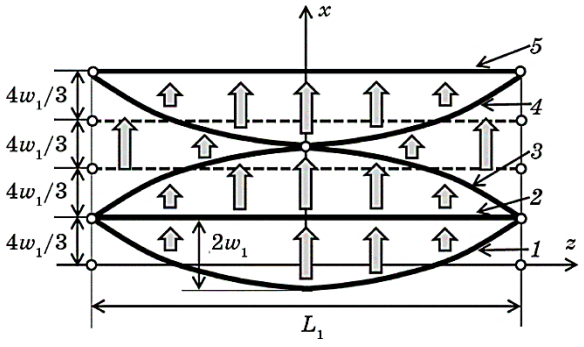

Fig. 4. The idealized process of the critical segment movement [36]. Grey arrows show the direction of movement of this segment.

where $\tilde{x} = 4w_1 / 3$ is the averaged forward displacement of the critical segment at which the maximum stress τ_{y1} is reached. The maximum stress is associated with the short-wavelength component of the shear-stress field in our case, because it dominates at the formation of a force barrier that the dislocation can overcome with the thermal activation assistance. This dependence is schematically shown in Fig. 5. The stress τ_{y1} required for the critical dislocation segment to overcome the short-wavelength component of the stochastic stress field without thermal activation will be equal to the stress acting on average from this component to this segment [3, 17]:

$$\tau_{y1} = s_1(2w_2)\sqrt{\frac{w_2}{w_1}}\sqrt{\frac{2w_1}{L_1}} = G\left(\frac{2}{\alpha\beta}\frac{w_1}{b}\right)^{1/3}\left(\frac{s_1(2w_2)}{G}\sqrt{\frac{w_2}{w_1}}\right)^{4/3} = \\ = A_1 G\left(\sum_{i=1}^{N}(\eta_i'^2 + \alpha_{s1}^2\delta_i^2)X_i\right)^{2/3}, \tag{13}$$

where

$$A_1 = \left(\frac{b^7 Q_1'^2}{32\alpha\beta w_1 w_2^2}\right)^{1/3} \tag{14}$$

for the alloy with f.c.c. lattice, and

$$A_1 = \left(\frac{b^7 Q_1'^2}{22.78\alpha\beta w_1 w_2^2}\right)^{1/3} \tag{15}$$

for the alloy with b.c.c. lattice. The average length L_1 of the critical

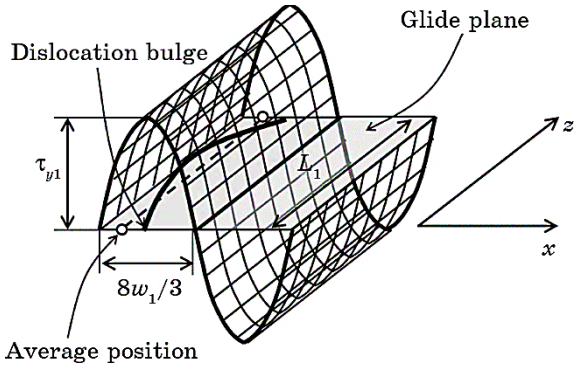

Fig. 5. Schematic presentation of the dependence of the stress acting on the critical segment in the glide plane on the averaged forward displacement of this segment x [36]. The average bulge on critical segment and its averaged position are also shown.

segment under acting short-wavelength component is [5, 36]:

$$L_1 = \left(\frac{\beta\Gamma}{s_1(2w_2)b\sqrt{w_2 / w_1}} \right)^{2/3} (2w_1)^{1/3}, \qquad (16)$$

where β is the coefficient depended on the shape of critical segment bulge ($\beta = 2\pi \approx 6.28$ for sinusoidal shape that confirmed by modelling [5]), Γ is the linear tension of the dislocation line ($\Gamma = \alpha G b^2$, where α is the coefficient less than 1/2).

It is more convenient to consider dependence (12) in terms of the force acting on the critical segment (Fig. 6). Then, the area under the curve will be measured in energy units. Point *1* at zero applied stress in Fig. 6 corresponds to state *1* in Fig. 4, point *2* corresponds to state *2* and so on, respectively. When an external stress τ is applied, the critical segment goes to the state with $x = x_s$. In order to overcome the force barrier from this position (pass through point *2*), it is necessary to provide the critical segment with additional energy ΔE, which is a function of τ. This energy can be obtained with the thermal activation assistance, which occurs due to thermal fluctuations. The probability of this event (a forward jump of the segment through the barrier) will depend on the energy ΔE and temperature T. At the same time, the critical segment will go to the state with $x = x_u$. This is a state of unstable equilibrium. In this case, the segment will quickly advance to the state with $x = x_2$ spontaneously. A backward jump from point with $x = x_2$ to

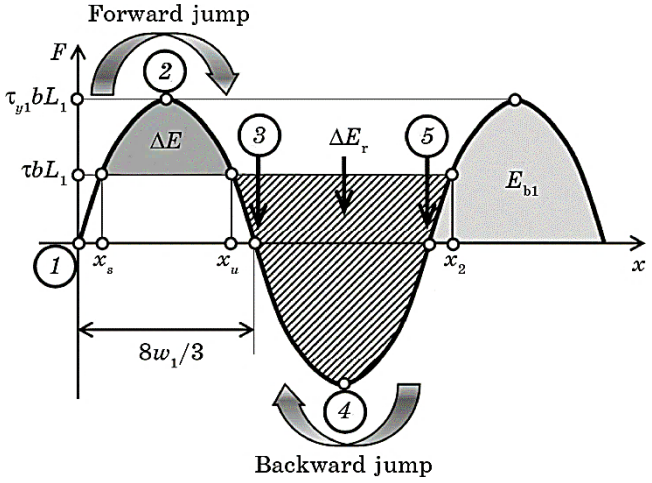

Fig. 6. Dependence of the force acting on the critical segment from the stochastic shear-stress field on the averaged forward displacement of this segment x [36]. Arrows show the directions of forward and reverse jumps through force barriers.

point with $x = x_u$ and further to point with $x = x_s$ is also possible. It is necessary to obtain energy ΔE_r through thermal activation for a backward jump. The probability of this jump will be determined by this energy and temperature T. Taking into account the probabilities of forward and backward jumps of critical segment, the strain rate can be expressed as [4]:

$$\dot{\varepsilon} = \dot{\varepsilon}_0 \left\{ \exp\left(-\frac{\Delta E}{k_B T} \right) - \exp\left(-\frac{\Delta E_r}{k_B T} \right) \right\}, \tag{17}$$

where $\dot{\varepsilon}_0$ is the pre-exponential factor, k_B is the Boltzmann constant. It should be noted that, for sinusoidal dependence (Fig. 6), we have [4]:

$$\Delta E = E_{b1}(1 - \tau / \tau_{y1})^{3/2}, \tag{18}$$

where the height of barrier from short-wavelength component in energy units [36]:

$$E_{b1} = \frac{16}{3\pi} b w_1 L_1 \tau_{y1} = \frac{25.398}{3\pi} (\beta\Gamma)^{1/3} b^{2/3} w_1^{4/3} w_2^{1/3} [s_1(2w_2)]^{2/3}. \tag{19}$$

Detailed analysis of area ratio in Fig. 6 results in

$$\Delta E_r = \Delta E + \pi E_{b1} \frac{\tau}{\tau_{y1}}. \tag{20}$$

Then from (17), (18) and (20) it can be derived the expression [36]:

$$\theta = (1 - \gamma)^{3/2} - (\theta / \lambda) \ln(1 - \exp(-\pi\lambda\gamma / \theta)), \tag{21}$$

where $\theta = T/T_0$, $\gamma = \tau/\tau_{y1}$, $\lambda = \ln(\dot{\varepsilon}_0 / \dot{\varepsilon})$ and

$$T_0 = \frac{E_{b1}}{k_B \ln(\dot{\varepsilon}_0 / \dot{\varepsilon})}. \tag{22}$$

Eq. (21) should be solved numerically to obtain the dependence $\gamma(\theta)$. If the appropriate values of $\dot{\varepsilon}_0 \approx 10^4$ s^{-1} and $\dot{\varepsilon}_0 \approx 10^{-3}$ s^{-1} are used [11], we have $\lambda = \ln(\dot{\varepsilon}_0 / \dot{\varepsilon}) \approx 16$. Then the equation (21) results in [36]:

$$\gamma = 1 - \theta^{2/3}, \; 0 \le \theta \le 0.9, \tag{23a}$$

$$\gamma = 4630 \exp(-12.35\theta), \; 0.9 < \theta. \tag{23b}$$

This result depends weakly on the values of $\dot{\varepsilon}_0$ and $\dot{\varepsilon}$, if the ratio $\dot{\varepsilon}_0 / \dot{\varepsilon}$ changes by an order of magnitude in one direction or another, since it is under the logarithm. The effect of backward jumps becomes noticeable only for $\theta > 0.9$, that is, at small applied stresses τ. At the

same time, the value γ quickly goes to zero. Practically we have $\gamma = 0$ at $\theta = 1.25$. Recall that in our analysis, τ is the applied stress, at which thermal activation assists overcoming the barriers from the short-wavelength component of the shear-stress field at a given strain rate and at a given temperature, essentially $\tau^* = \tau$.

The existence of the long-wavelength component of the shear-stress field, the calculation of which is shown in Ref. [33], was proved by modelling dislocation motion in Ref. [5]. The stress required for athermal overcoming of the force barrier from the long-wavelength component is [36]

$$\tau_{y2} = s_2(2w_2)\sqrt{\frac{2w_2}{L_2}} = G\left(\frac{2}{\alpha\beta}\frac{w_2}{b}\right)^{1/3}\left(\frac{s_2(2w_2)}{G}\right)^{4/3} = \\ = A_2 G\left(\sum_{i=1}^{N}(\eta_i'^2 + \alpha_{s2}^2\delta_i^2)X_i\right)^{2/3}, \tag{24}$$

where

$$A_2 = \left(\frac{b^7 Q_2'^2}{32\alpha\beta w_2^3}\right)^{1/3} \tag{25}$$

for the alloy with f.c.c. lattice, and

$$A_2 = \left(\frac{b^7 Q_2'^2}{22.78\alpha\beta w_2^3}\right)^{1/3} \tag{26}$$

for the alloy with b.c.c. lattice. The average length L_2 of the critical segment under acting long-wavelength component can be determined by analogy like L_1 [5]:

$$L_2 = \left(\frac{\beta\Gamma}{s_2(2w_2)b}\right)^{2/3}(2w_2)^{1/3}. \tag{27}$$

Now we can take $\tau_\mu = \tau_{y2}$. The height of barrier from long-wavelength component in energy units can be found by analogy as for short-wavelength component using Eq. (19), if necessary replacements will be made [36]:

$$E_{b2} = \frac{16}{3\pi} b w_2 L_2 \tau_{y2} = \frac{25.398}{3\pi}(\beta\Gamma)^{1/3} b^{2/3} w_2^{5/3}(s_2(2w_2))^{2/3}. \tag{28}$$

Eqs. (11) and (23) lead to the temperature dependence of the yield strength of a multicomponent alloy in the form of a single-phase concentrated solid solution, taking into account only solid solution strengthening and two components of the shear-stress field in the glide

plane, in the form [36]:

$$\sigma_y = M\{\tau_P + \tau_{y1}[1 - (T / T_0)^{2/3}] + \tau_{y2}\},\ 0 \le T \le 0.9T_0\,, \quad (29a)$$

$$\sigma_y = M\{\tau_P + 4630\tau_{y1}\exp(-12.35T / T_0) + \tau_{y2}\},\ T > 0.9T_0\,. \quad (29b)$$

However, the characteristic stresses τ_{y1} and τ_{y2} can depend on temperature due to the temperature dependence of the shear modulus G. The existence of a 'plateau' on the temperature dependence of the yield strength at high temperatures, when the yield strength remains constant in a certain temperature range, proves that the drop in the shear modulus with temperature is necessarily compensated for, in some way, for example, by an increase in the crystal lattice distortion as the temperature increases [25]. That is, the drop in the shear modulus should actually be compensated by an increase in $s_1(2w_2)$ and $s_2(2w_2)$, which depend on lattice distortion. This allows to assume that the products of the shear modulus and the factors associated with $s_1(2w_2)$ and $s_2(2w_2)$ in Eqs. (13) and (24) do not depend on temperature [36]. Thus, it is enough to calculate them at some temperature and consider them approximately the same for all other temperatures.

3. RESULTS AND DISCUSSION

3.1. Characteristics of Shear-Stress Field in Glide Plane in the CrCoNiFeMn Alloy

The method of determining the standard deviations and correlation lengths of the short- and long-wavelength components of the stochastic shear-stress field in the glide plane needs verification. To do this, it must be applied to a multicomponent alloy, the above-mentioned characteristics of which are known from other sources. Multicomponent CrCoNiFeMn alloy was chosen to verify the method. This alloy is a substitutional solid solution having an f.c.c. lattice. The parameters s_1, w_1, s_2 and w_2 for this alloy were determined in [33] by another method from the analysis of shear-stresses' distributions in the glide plane, which were calculated by the method of direct summation of contributions from solute atoms. The input parameters for calculation were taken as in [33]: shear modulus $G = 81$ GPa, bulk modulus $K = 176$ GPa, Poisson's ratio $\nu = 0.3$, Burgers vector $b = 0.25$ nm, atomic volume $V_a = 0.011$ nm^3. Atomic size misfits and elastic modulus misfits for component atoms are given in Table 1 [33]. The critical distance of approximately 4.75 nm was determined, at which the contribution to the shear stress from the solute atom should still be taken into account [24, 33]. Therefore, in the sums P_1', Q_1', P_1'', Q_1'', P_2', Q_2', P_2'', Q_2'' it is necessary to take into account only contributions from atoms that are at a dis-

TABLE 1. Atomic-sizes' misfits δ_i and elastic-moduli misfits η_i for component atoms used for the calculation of main parameters of shear-stress field in the CrCoNiFeMn alloy [35].

Component	i	X_i	δ_i	η_i
Cr	1	0.2	0.010077	0.290837
Co	2	0.2	0.001747	–0.13433
Ni	3	0.2	0.004622	–0.12114
Fe	4	0.2	0.004674	–0.04529
Mn	5	0.2	–0.02244	–0.05755

tance less than or equal to 4.75 nm from the point with coordinates x_u and z_u.

The dependences of the parameters s_1, w_1, s_2 and w_2 on the x_u coordinate in the range of $0 \le x_u \le b$ were determined by equations (6) and (10) at $\Delta z = 1.94$ nm for various characteristic values of the z_u coordinate from the range of $0 \le z_u \le b(3)^{1/2}$ for the CrCoNiFeMn alloy [33, 35, 36]. Dependences s_1 and w_1 are symmetrical with respect to $x_u = 0.125$ nm, because this is the distance between the atomic planes that are perpendicular to the Burgers vector in the f.c.c. lattices in our chosen alloy. The atoms are located along a straight line parallel to the Burgers vector with a step equal to the absolute value of this vector, *i.e.* 0.25 nm. The parameters $s_1 = 180$ MPa and $w_1 = 0.38$ nm averaged over x_u and z_u correlate well with the average values $s_1 = 191$ MPa and $w_1 = 0.38$ nm, which were determined in Ref. [33] from the analysis of shear-stresses' distributions in the glide plane. It should also be noted that the ranges of minimum–maximum values of 165–208 MPa for s_1 and of 0.21–0.54 nm for w_1 in the proposed method also correlate well with similar ranges of 166–234 MPa and 0.32–0.48 nm determined in [33]. Dependences s_2 and w_2 demonstrate the practical independence of these parameters on x_u and z_u [35]. This is due to the fact that s_2 and w_2 are determined by atoms farther from the glide plane and from the dislocation core. The averaged parameters of $s_2 = 71$ MPa and $w_2 = 1$ nm also correlate well with the average values of $s_2 = 72$ MPa and $w_2 = 0.97$ nm, which were determined in [33].

A certain combination of atomic size misfits and elastic modulus misfits is used to characterize the general lattice distortion in [37]:

$$\chi = \left(\sum_{i=1}^{N} (\eta_i'^2 + \alpha_0^2 \delta_i^2) X_i\right)^{2/3}, \tag{30}$$

where α_0 is the constant that equal to 16 for the edge dislocations [20, 24, 30, 37]. This parameter is called the average distortion of crystal lattice in [24]. Statistical method of the determination of the standard

deviations of the shear-stress field leads to similar combinations in (13) and (24), which can be called the effective lattice distortions for the short- and long-wavelength components, respectively [35]:

$$\chi_{s1} = (\sum_{i=1}^{N} (\eta_i'^2 + \alpha_{s1}^2 \delta_i^2) X_i)^{2/3} \text{ and } \chi_{s2} = (\sum_{i=1}^{N} (\eta_i'^2 + \alpha_{s2}^2 \delta_i^2) X_i)^{2/3}. \quad (31)$$

Equations (31) differ from (30) because instead of α_0 they contain α_{s1} and α_{s2}, which can be calculated by equations (7). These parameters averaged over the characteristic region $0 \le x_u \le b$ and $0 \le z_u \le b(3)^{1/2}$ are $\alpha_{s1} = 39$ and $\alpha_{s2} = 107$, and the corresponding parameters $\chi_{s1} = 0.36$ and $\chi_{s2} = 1.32$ for the CrCoNiFeMn alloy. Note that in this case $\chi = 0.14$. In essence, the constant α_0 is the ratio of the force of dislocation interaction with a solute atom, caused by atomic size misfit, to the force of interaction caused by elastic modulus misfit [32]. The farther the solute atom is located from the glide plane, the greater this ratio. This is explained by the fact that the force of interaction, caused by elastic modulus misfit, decreases with the distance from the glide plane faster than the force, caused by atomic size misfit. If only the solute atoms nearest to the glide plane are taken into account, then this ratio cannot be less than 16 for an edge dislocation. This determines that the constant $\alpha_0 = 16$ [20, 24, 30, 37]. The parameters α_{s1} and α_{s2} have the same sense as α_0. Their larger values are due to the fact that solute atoms farther from the glide plane than in the calculation of α_0 are taken into account. At the same time, α_{s2} is greater compared to α_{s1}, because atoms farther from the glide plane participate when forming the long-wavelength component of the stress field in comparison with forming the short-wavelength component. Thus, the method considered in this paper proposes the use of different effective lattice distortions to determine the main parameters of the short- and long-wavelength components of the shear-stress field.

Athermal component of solid solution strengthening was considered in [20, 35] as

$$\Delta\sigma_\mu = AG\chi, \quad (32)$$

where A is the empirical constant. Average value of 0.0026 ± 0.0005 was determined for this constant by experimental data treatment for many alloys with f.c.c. lattice. On other hand, we have $\Delta\sigma_\mu = M\tau_{y2}$ [36]. Eqs. (24), (31) and (32) result in

$$A = MA_2\chi_{s2} / \chi, \quad (33)$$

where A_2 is determined by Eq. (25) [35]. In our case, we have $A_2 = 0.000133$ for the CrCoNiFeMn alloy. Then, the constant can be calculated as $A = 0.0038$ according to Eq. (33). This is comparable with

the value given in Ref. [20]. It should be noted that the values of χ_{s2} and A_2 will also depend on the Poisson's ratio of the alloy due to the stress-tensor components at the solute atom location. The larger Poisson's ratio, the larger χ_{s2} and A_2. That is, each alloy may have its own individual value of A_2. The constant A was calculated for one specific alloy in this work, and it was determined by averaging data for many alloys, each of which had its own Poisson's ratio, in [20]. Under such circumstances, these two values of the constant A cannot completely match. They will necessarily be different from each other. Nevertheless, their comparability proves that the statistical method proposed here gives at least realistic results. It can also be concluded that the constant A for each alloy has its own individual value. There is no single constant A for all alloys. The sums P_1', Q_1', P_1'', Q_1'', P_2', Q_2', P_2'', Q_2'', which determine the main parameters of the shear-stress field, are also individual for each alloy. It should be noted that they are not random quantities like the shear stresses in the glide plane, which depend on the specific random arrangement of various solute atoms. This is one of the advantages of the proposed method in comparison with the method of direct summation of contributions from solute atoms.

3.2. Temperature Dependence of Yield Strength of CrCoNiFeMn Alloy

A multicomponent CrCoNiFeMn alloy was also used to model the temperature dependence of the yield strength taking into account the short- and long-wavelength components of the stochastic shear-stress field in the glide plane. The input and calculated parameters of modelling are listed in Table 2. An important parameter is also the coefficient $\alpha = 0.123$, which determines the linear tension of the dislocation line in the CrCoNiFeMn alloy [12]. The Peierls–Nabarro stress, *i.e.*, the frictional stress of the lattices of the virtual matrix-solvent, can be estimated as for metals with f.c.c. lattice and taken, for example, to be approximately $\tau_P = 3$ MPa [4]. The temperature dependence of the yield strength in this material taking into account only solid solution strengthening is shown in Fig. 7. The solid line corresponds to calculations using equations (29) for the averaged main parameters of the shear-stress field, which are given in Table 2. Circles, triangles, and squares are experimental data taken from the literature [38–40]. The grey band corresponds to the band of possible theoretical yield strengths, taking into account the inaccuracy of the main parameters determination. Experimental values from different sources correlate well with each other and with the modelled dependence. They demonstrate clearly 'plateau' at temperatures above approximately 650 K. The theoretical dependence smoothly transitions to this 'plateau'. There is a deviation of the calculated dependence from the experimental values in the region of very low temperatures.

TABLE 2. The input and calculated parameters of modelling the temperature dependence of yield strength of the CrCoNiFeMn alloy [36].

G, GPa	81	$s_1(2w_2)$, MPa	180	$s_2(2w_2)$, MPa	71
α	0.123	w_1, nm	0.38	w_2, nm	1
τ_P, MPa	3	L_1, nm	12.97	L_2, nm	45.96
b, nm	0.25	τ_{y1}, MPa	70.69	τ_{y2}, MPa	14.81
T_0, K	664	E_{b1}, eV	0.92	E_{b2}, eV	1.8

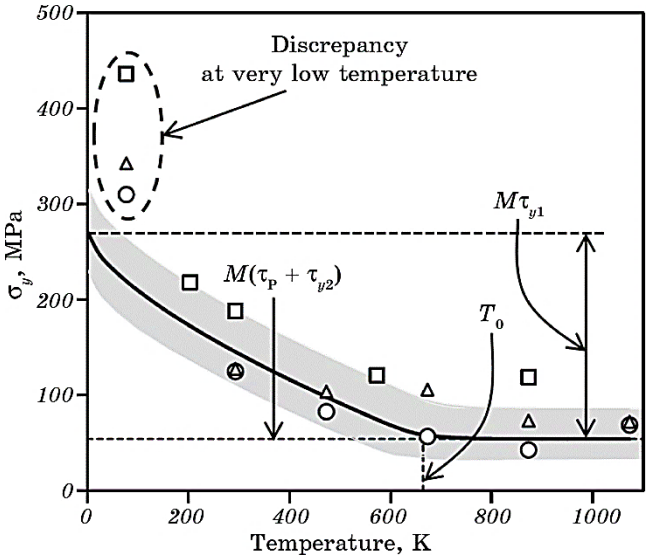

Fig. 7. Temperature dependence of the yield strength of the CrCoNiFeMn alloy taking into account only solid solution strengthening [36]. The solid line is a calculation using equations (29) for the averaged main parameters of the shear-stress field, which are presented in Table 2. Circles, triangles, and squares are experimental values taken from [38], [39], and [40], respectively. The grey band corresponds to the band of possible theoretical yield strengths, taking into account the inaccuracy of the main parameters determination.

The stochastic shear-stress field in the glide plane was not calculated at all in work [11], that is, its short- and long-wavelength components were not determined as well. Nevertheless, a force barrier of a sinusoidal profile was considered similarly to our work as an obstacle for the dislocation motion. The height of this barrier was determined on the basis of the interaction energies of solute atoms with dislocations calculated from first principles [11]. The temperature dependence of the yield strength of the CrCoNiFeMn alloy was obtained from the analysis of dislocation overcoming of this sinusoidal force barrier

in this paper. It is obvious that the athermal component of the yield strength associated with solid solution strengthening and with long-wavelength component of the shear-stress field was not considered at all in [11].

In fact, the theoretical temperature dependence from [11] does not have a 'plateau' demonstrated by experimental data [38–40]. Instead, this dependence smoothly goes to zero without a 'plateau'. Perhaps that is why the theoretical temperature dependence and experimental data from [38] are compared in [11] only up to a temperature of 673 K, and this is only the very beginning of the 'plateau' for the CrCoNiFeMn alloy. The 'plateau' exists for this alloy at least from 670 K to 1073 K. In addition, the theoretical temperature dependence from [11] at 673 K is slightly below the experimental value. This theoretical dependence will be even lower at higher temperatures, when the experimental data show a 'plateau', that is, an almost constant value of the yield strength. On the other hand, this dependence practically coincides with the experimental value from [38] at 293 K, but is lower than the value from [40] at this temperature. Instead, the theoretical temperature dependence of the yield strength of the CrCoNiFeMn alloy, which was calculated in our paper, is higher than the similar dependence from the paper [11]. This better correlates with the entire set of experimental data from Refs. [38–40], except for the range of very low temperatures. Such discrepancy is explained by a possible change in the linear tension of the dislocation line in this temperature range in [11]. However, this assumption requires further research. It should also be added that at sufficiently high temperatures, which are not considered in this work, the yield strength will no longer be on the 'plateau', but will start to decrease sharply due to the action of other mechanisms of plastic deformation instead of dislocation gliding.

The main advantage of our approach is that it takes into account the athermal component of the yield strength associated with solid solution strengthening. This component can be associated with the long-wavelength component of the stochastic stress field in the glide plane. In this case, it is possible to calculate the theoretical 'plateau' stress almost exactly. On the other hand, if the force barrier for the dislocation motion, which can be overcome with the thermal activation assistance and which determines the course of the temperature dependence of the yield strength, is connected with the short-wavelength component, then the temperature of the beginning of the 'plateau' can be fairly accurately predicted (T_0 in Table 2). This cannot be done within the framework of the model from work [11]. The activation volume at 293 K, calculated from our theoretical temperature dependence according to the method from [12], is equal to $V = 147b^3$. This correlates well with the value $2w_1L_1b \approx 153b^3$ obtained from the geometrical parameters of the average dislocation bulge for the CrCoNiFeMn alloy

(Table 2). On the other hand, this value has one order of magnitude with the value $\sim 350b^3$ for this alloy, which was determined by the experimental method in [41].

4. CONCLUSION

Atomic size misfits and elastic modulus misfits at the crystal lattice sites can be considered as discrete random variables with a mathematical expectation equal to zero and a certain non-zero variance. Analytical expressions for the standard deviations and correlation lengths of the short- and long-wavelength components of the stochastic shear-stress field created by solute atoms in the glide plane in a multicomponent alloy were obtained from the variance definition of these random variables. The developed method was verified by calculating the main parameters of shear-stress field for the CrCoNiFeMn alloy. The calculated parameters were well correlated with similar parameters determined from the analysis of shear-stresses' distributions in the glide plane, which were calculated by the method of direct summation of contributions from solute atoms. It was found that it is possible to define two different effective distortions of crystal lattice, which cause short- and long-wavelength components of the stress field, respectively. In addition, it was established that there is no single empirical constant for all alloys to determine the yield strength using the shear modulus and the average lattice distortion. However, it is possible to calculate the yield strength of a specific multicomponent alloy using the main parameters of the shear-stress field, which are determined by the method considered in this paper.

The periodic lattice potential, short- and long-wavelength components of the stochastic shear-stress field in the glide plane determine the yield strength of a multicomponent alloy taking into account only solid solution strengthening. The force barriers from the short- and long-wavelength components are described using the main parameters of the shear-stress field. The force barrier for the dislocation motion from the short-wavelength component is dominant in a multicomponent alloy, which is a concentrated solid solution. In this case, the beginning of dislocation motion is determined by overcoming this barrier with the assistance of applied stress and thermal activation. The effect of barriers from the periodic lattice potential and the long-wavelength component on the yield strength can be taken into account by constant terms that do not depend on temperature. This is possible because these barriers are quite low in comparison with the barrier from the short-wavelength component in a concentrated solid solution. The temperature dependence of the yield strength of a multicomponent alloy in a wide temperature range can be determined using thermal activation analysis of overcoming barriers from the short-wavelength

component, taking into account the probability of forward and backward jumps through the barriers and the constant stresses that take into account the barriers from the periodic lattice potential and long-wavelength component. Effect of solute atoms located farther from the glide plane on yield strength cannot be neglected because they create long-wavelength component of the shear-stress field. The temperature dependence of the yield strength calculated in this way describes well the region of the high-temperature 'plateau'. This dependence, calculated for the CrCoNiFeMn alloy, also correlates well with the corresponding experimental data for this alloy.

REFERENCES

1. D. B. Miracle and O. N. Senkov, *Acta Mater.*, **122**: 448 (2017).
2. E. P. George, W. A. Curtin, and C. C. Tasan, *Acta Mater.*, **188**: 435 (2020).
3. F. R. N. Nabarro and P. B. Hirsch, *The Physics of Metals* (Cambridge: Cambridge University Press: 1976), p. 152.
4. A. S. Argon, *Strengthening Mechanisms in Crystal Plasticity* (Oxford: Oxford University Press: 2008).
5. M. Lugovy, D. Verbylo, and M. Brodnikovskyy, *Uspikhy Materialoznavstva*, Nos. 4/5: 36 (2022) (in Ukrainian).
6. R. Labusch, *Czech. J. Phys. B*, **31**: 165 (1981).
7. G. Leyson, W. Curtin, L. Hector, and C. F. Woodward, *Nature Mater.*, **9**: 750 (2010).
8. G. P. M. Leyson, L. G. Hector, and W. A. Curtin, *Acta Mater.*, **60**, No. 9: 3873 (2012).
9. G. P. M. Leyson and W. A. Curtin, *Phil. Mag.*, **93**, Iss. 19: 2428 (2013).
10. G. P. M. Leyson and W. A. Curtin, *Modelling Simulation Mater. Sci. Eng.*, **24**: 065005 (2016).
11. C. Varvenne, A. Luque, and W. A. Curtin, *Acta Mater.*, **118**: 164 (2016).
12. C. Varvenne, G. P. M. Leyson, M. Ghazisaeidi, and W. A Curtin, *Acta Mater.*, **124**: 660 (2017).
13. W. G. Nöhring and W. A. Curtin, *Scripta Mater.*, **168**: 119 (2019).
14. G. Bracq, M. Laurent-Brocq, C. Varvenne, L. Perrière, W. A. Curtin, J.-M. Joubert, and I. Guillot, *Acta Mater.*, **177**: 266 (2019).
15. Y. Hu, B. A. Szajewski, D. Rodney, and W. A. Curtin, *Modelling Simulation Mater. Sci. Eng.*, **28**: 015005 (2020).
16. M. Zaiser, *Phil. Mag. A*, **82**, No. 15: 2869 (2002).
17. J.-H. Zhai and M. Zaiser, *Mater. Sci. Eng. A*, **740–741**: 285 (2019).
18. G. Péterffy, P. D. Ispánovity, M. E. Foster, X. Zhou, and R. B. Sills, *J. Mater. Sci.: Mater. Theory*, **4**: 6 (2020).
19. R. Pasianot and D. Farkas, *Computational Mater. Sci.*, **173**: 109366 (2020).
20. M. Lugovy, V. Slyunyayev, and M. Brodnikovskyy, *Progress in Natural Sci.: Mater. Int.*, **31**: 95 (2021).
21. M. Lugovy, V. Slyunyayev, M. Brodnikovskyy, and S. Firstov, *Ehlektronnaya Mikroskopiya i Prochnost' Materialov*, Iss. 23: 3 (2017) (in Ukrainian).
22. M. Lugovy, V. Slyunyayev, and M. Brodnikovskyy, (2019). *Ehlektronnaya Mikroskopiya i Prochnost' Materialov*, Iss. 25: 26 (2019) (in Russian).

23. M. Lugovy, D. Verbylo, and M. Brodnikovskyy, *Uspikhy Materialoznavstva*, No. 2: 19 (2021) (in Ukrainian).
24. M. Lugovy, D. Verbylo, and M. Brodnikovskyy, *Uspikhy Materialoznavstva*, No. 3: 24 (2021) (in Ukrainian).
25. S. O. Firstov and T. G. Rogul, *Metallofiz. Noveishie Tekhnol.*, **44**, No. 1: 127 (2022) (in Ukrainian).
26. A. V. Podolskiy, E. D. Tabachnikova, V. V. Voloschuk, V. F. Gorban, N. A. Krapivka, and S. A. Firstov, *Mater. Sci. Eng. A*, **710**: 136 (2018).
27. S. O. Firstov, T. G. Rogul, N. A. Krapivka, and S. I. Chugunova, *Metallofiz. Noveishie Tekhnol.*, **40**, No. 2: 219 (2018) (in Russian).
28. S. O. Firstov and T. G. Rogul, *Metallofiz. Noveishie Tekhnol.*, **39**, No. 1: 33 (2017) (in Russian).
29. L. A. Gypen and A. Deruyttere, *J. Mater. Sci.*, **12**: 1028 (1977).
30. I. Toda-Caraballo, *Scripta Mater.*, **127**: 113 (2017).
31. U. F. Kocks, A. S. Argon, and M. F. Ashby, *Progress Mater. Sci.*, **19**: 110 (1975).
32. R. L. Fleischer, *Acta Metallurgica*, **11**: 203 (1963).
33. M. Lugovy, D. Verbylo, and M. Brodnikovskyy, *Uspikhy Materialoznavstva*, Nos. 4/5: 12 (2022) (in Ukrainian).
34. G. Gremaud, *Mater. Sci. Eng. A*, **370**: 191 (2004).
35. M. Lugovy, D. Verbylo, and M. Brodnikovskyy, *Uspikhy Materialoznavstva*, No. 7: 3 (2023) (in Ukrainian).
36. M. Lugovy, D. Verbylo, and M. Brodnikovskyy, *Uspikhy Materialoznavstva*, No. 6: 15 (2023) (in Ukrainian).
37. R. Labusch, *phys. status solidi (b)*, **41**, Iss. 2: 659 (1970).
38. F. Otto, A. Dlouhy, C. Somsen, H. Bei, G. Eggeler, and E. P. George, *Acta Mater.*, **61**: 5743 (2013).
39. A. Gali and E. P. George, *Intermetallics*, **39**: 74 (2013).
40. S. J. Sun, Y. Z. Tian, H. R. Lin, X. G. Dong, Y. H. Wang, Z. J. Wang, and Z. F. Zhang, *J. Alloys Compd.*, **806**: 992 (2019).
41. G. Laplanche, J. Bonneville, C. Varvenne, W. A. Curtin, and E. P. George, *Acta Mater.*, **143**: 257 (2018).